RSC Advances

PAPER

View Article Online
View Journal | View Issue

Check for updates

Cite this: *RSC Adv.*, 2024, **14**, 24185

Optimizing photovoltaic performance of squaraine derivative dyes: a DFT study on different anchoring groups†

Giuseppe Consiglio, *[a] Adam Gorczyński, [b] Guido Spoto,[c] Salvatore Petralia [d] and Giuseppe Forte *[d]

In this study, we designed squaraine-based dyes with a 2-amino pyrrole donor unit and acene groups like anthracene and pentacene. These dyes incorporate three different electron-withdrawing groups – cyanoacrylate (**A1**), phosphonate (**A2**) and boronic acid (**A3**) – as linkers to the TiO_2 semiconductor. The spectroscopic, electronic and photochemical properties of these compounds were investigated using density functional theory (DFT) and time-dependent density functional theory (TDDFT) simulations. Compared to the squarylium dye, **SQD**, the UV-vis data indicate excellent absorption especially for pentacene-based dyes, which extended beyond 920 nm, enhancing the panchromatic effect. The calculated excited-state lifetimes of these dyes were notably longer than **SQD**, particularly for those containing pentacene and either **A1** or **A2** withdrawing groups, with lifetimes approximately four times longer. In contrast, boronic acid derivatives had shorter excited-state lifetimes, hindering charge transfer. Simulations suggest all sensitizers can inject electrons into TiO_2 and be efficiently regenerated by electron transfer from the electrolyte. The best results were achieved with pentacene and **A1** or **A2** as linkers, notably **A1** dyes achieve superior short circuit photocurrent, J_{sc}, and power conversion efficiency, PCE, with over 50% improvement compared to **SQD**. Phosphonate derivatives exhibited the highest energy adsorption on TiO_2 while still achieving significant open-circuit voltage, V_{oc}, J_{sc}, and PCE values. After surface adsorption, all dyes displayed efficient electron recovery, with HOMO levels significantly dropping below −4.8 eV. Our study demonstrates that computational design can significantly enhance experimental work, offering valuable insights to improve dye design and boost the performance of dye-sensitized solar cells.

Received 22nd July 2024
Accepted 27th July 2024

DOI: 10.1039/d4ra05322b

rsc.li/rsc-advances

Open Access Article. Published on 02 August 2024. Downloaded on 2/7/2026 6:10:27 PM.
This article is licensed under a Creative Commons Attribution-NonCommercial 3.0 Unported Licence.

1. Introduction

Solar energy, thanks to its main characteristics such as abundance and renewability, has the potential to satisfy global energy demand while respecting the environment. By means of photovoltaics (PV) it is possible to directly convert sunlight into electricity, through solar cells. Traditional ones, made of crystalline silicon, represent the most widespread technology, but have some limitations, including the high production cost and poor flexibility. Dye-sensitized solar cells, DSSCs, also referred to as Gratzel cells, are a well-established solar energy conversion technology. They offer a promising alternative to conventional silicon-based solar cells. A key component of DSSCs is the photosensitizer, which is crucial for photon absorption and initiating the charge separation process.[1] Photosensitizers are generally divided into three primary categories: ruthenium(II) complexes,[2–6] zinc(II) porphyrin derivatives,[7–13] and metal-free organic dyes. Notably, metal-free organic dyes have gained substantial attention because of their economical production processes and reduced environmental impact. In recent years, the conversion efficiency of organic solar cells has been significantly improved, as have their stability and durability. In order to harvest the entire solar spectrum as efficiently as possible, organic dye molecules that absorb strongly in the near-infrared regions, NIR, and infrared regions are looked-for. Among several types of sensitizers, squaraine dyes are attracting many attentions.[14] Squaraine dyes are fascinating molecules characterized by an electron deficient four membered aromatic ring derived from squaric acid. Probably, the most important reason of increasing attention of squaraine dyes is that they have intense and broad absorption in the visible and NIR regions. Furthermore, they possess very high optical densities and molar

[a]*Department of Chemical Science University of Catania, Via S. Sofia 64, 95125, Italy. E-mail: giuseppe.consiglio@unict.it*

[b]*Faculty of Chemistry, Adam Mickiewicz University, Uniwersytetu Poznańskiego 8, 61-614 Poznań, Poland*

[c]*InfoBiotech S.r.l, Via del Bersagliere, 45, 90143 Palermo, Italy*

[d]*Department of Drug Science and Health University of Catania, Via S. Sofia 64, 95125, Italy. E-mail: gforte@unict.it*

† Electronic supplementary information (ESI) available. See DOI: https://doi.org/10.1039/d4ra05322b

© 2024 The Author(s). Published by the Royal Society of Chemistry

Open Access Article. Published on 02 August 2024. Downloaded on 2/7/2026 6:10:27 PM. This article is licensed under a Creative Commons Attribution-NonCommercial 3.0 Unported Licence.

extinction coefficients.[14,15] In previous papers, dye-sensitized solar cells, DSSCs, have been prepared through the insertion of thiophene, pyrrole, thiazole, and indole moieties into squaraine dyes.[16–18] Intramolecular charge transfer (ICT) and light harvesting could lead to increase of efficiency, especially through bridge elongation, and/or push–pull strategies.[19–24] Rajbhoj *et al.*[25] have investigated the structural, electronic, photo-electrochemical, and charge transport properties of two indole-based squaraine chromophores (SQ1 and SQ2) by means of density functional theory (DFT). The effect of –COOH and –OCH_3 substituents on SQ1 and SQ2 dyes was studied. They found that methoxy group rises while carboxylic one decreases the energies of HOMOs and LUMOs, leading to a greater open-circuit voltage, V_{oc}, for SQ1 and SQ2 compared to dye-nitro and *cis*-SQ dyes. Recently, Yang *et al.* reported a novel D_1–A–D_2 type indole-based squaraine dye containing dithieno[3,2-*b*:2′,3′-*d*] thiophene (DTT). In contrast with the standard D_1–A–D_2 type squaraine dye without DTT, they obtained a red shift of the absorption band, a lower optical bandgap, and a deeper HOMO/LUMO energy level, which is attributed to its larger planar molecular geometry.[26] As π-extended dye sensitizers usually have long dipole moment, dipole–dipole interactions between the dye molecules are facilitated on the semiconductor surface. This dye–dye interaction is responsible of absorption broadening, but the role of the assembled molecules to the power conversion is poor. Such self-assembly of sensitizers through dye–dye interactions on the TiO_2 surface diminishes the DSSC performance, even if it helps the broadening of the absorption profile of the sensitizing dye.[27] Punitharasu *et al.*[28] have designed a conjugated *cis* unsymmetrical squaraine dyes, with carboxylic and cyanoacetic moieties as anchoring groups, and with steric and electronic features that control self-assembly and panchromatic light absorption. The presence of out-of-plane long alkyl chains on sp^3 carbon and coplanar *N*-alkyl chain played a central role in controlling the aggregation of the dye molecules on the surface. Furthermore, the *cis*-squaraine moiety extends the conjugation, resulting in panchromatic incident photon-to-current conversion efficiency, IPCE, profile and NIR absorption. Panchromatic absorption in the range 300–850 nm is central for obtaining high-performance organic-based DSSCs. Unfortunately, attaining it with a single organic molecule is very hard, as only a few examples have been published.[29–34] A possible solution is a co-sensitization of different molecules which display absorption in different portions of the UV-NIR range.[35–42] For this purpose, a molecular-engineering approach is essential to get organic molecules with selective absorptions and combine them together to attain panchromatic absorption. Recently, co-sensitization was used to obtain panchromatic absorption over the whole visible spectrum and to get a high performance DSSCs.[43] An interesting example of panchromatic absorption using three different organic molecules, have been recently reported. In this paper,[44] co-sensitization of dye Y1, dye TP_2A, and a squaraine based dye HSQ4 gave panchromatic absorption in the 300–820 nm range. The Y1 + TP_2A + HSQ4 dyes DSSC shows high values of short circuit photocurrent, J_{sc} open-circuit voltage and power conversion efficiency, PCE. The IPCE spectrum of the DSSC indicates an improved efficacy of the injection compared to each single dye and TP_2A + HSQ4 dyes. This DSSC shows a panchromatic absorption with an IPCE >70% in the range 300–820 nm, suggesting their usage in indoor applications. In recent computational research, our group examined the opto-electronic features and efficiency of a new class of D–π–A dyes for DSSC. The π-bridge included a linear carbon chain, with cyanoacrylic acid functioning as the acceptor and 2-amino pyrrole serving as the donor group.[45,46] The top calculated performance yielded a PCE of 21.29%. We further analyzed the charge transfer efficiency of the 2-amino pyrrole donor group in conjunction with various electron-attracting groups. Pairing 2-amino pyrrole with the innovative electron-attracting group pyrimidin–pyridinium salt, improved characteristics over groups like phenothiazine and cyanoacrylic acid.[47] Nevertheless, UV-vis spectra showed a limitation at about 550 nm causing significant solar energy loss. To extend absorption and design panchromatic-active sensitizers in the far-red and near-infrared regions, we added acene groups into the donor segment, motivated by previous research indicating that acenes broaden and red-shift absorption. This modification resulted in new structures with panchromatic characteristics, with absorption extending into the near IR region and outstanding predicted PCE values of about 30%.[48] A major challenge in further improving the efficiencies of DSSCs is their inadequate absorption in the far-red/NIR spectrum. Visible light, spanning 350–700 nm, makes up around 45% of the solar energy that reaches the earth's surface, while red/NIR light, covering 600–1000 nm, comprises roughly 25%. To increase the current output of these devices, it is essential to design materials and molecules that can effectively utilize the entire solar spectrum. Therefore, converting NIR radiation into electricity is a key objective in the advancement of DSSC technology.[49,50] In this work, we build upon previous research to design derivatives of squaraine, aiming to enhance their performance. Specifically, we modified the donor group by introducing the 2-amino pyrrole derivative, along with acene group such as anthracene and pentacene. Additionally, we considered cyanoacrylate (**A1**) and two others widely used acceptor groups for TiO_2 anchoring, the phosphonate group (**A2**) and a boronic acid derivative (**A3**), to evaluate their potential advantages.[51–56] The resulting structures are shown in Fig. 1. Our ultimate goal is to contribute to the ongoing efforts to achieve sustainable and efficient solar energy conversion technologies.

2. Methods

Molecular simulations of the investigated dyes were performed using the Gaussian 16 program package.[57] The geometries were fully optimized utilizing the B3LYP functional with the 6-311+G(2d,p) basis set. To compute UV-vis spectra, the TD-DFT approach with the same basis set was applied, focusing on the lowest 15 singlet–singlet transitions. The CAM-B3LYP functional was chosen due to its reliability in producing UV-vis spectrum that closely match experimental data for the squarylium dye III, **SQD**, considered as reference compound.[58,59] Additionally, for comparison, ωB97XD and M062X functionals

 © 2024 The Author(s). Published by the Royal Society of Chemistry

Open Access Article. Published on 02 August 2024. Downloaded on 2/7/2026 6:10:27 PM.
This article is licensed under a Creative Commons Attribution-NonCommercial 3.0 Unported Licence.

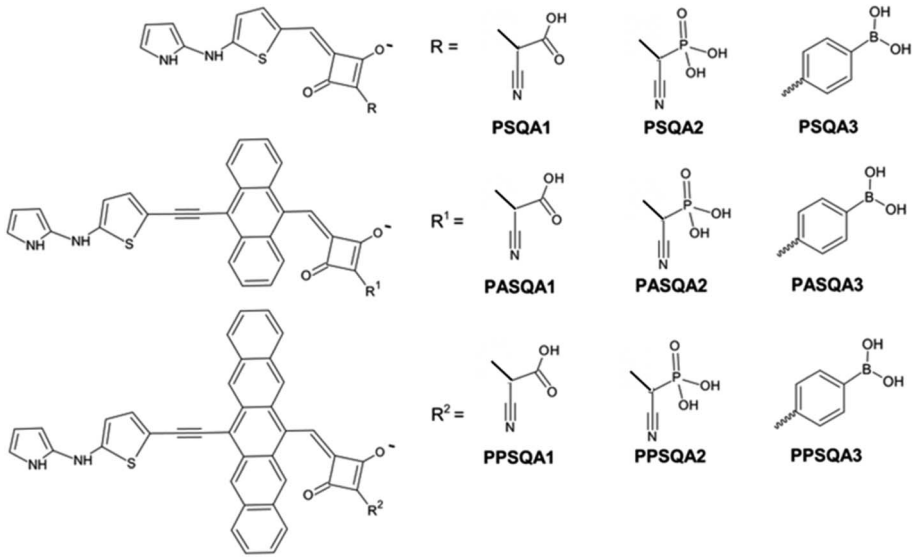

Fig. 1 Molecular structure of the designed dyes.

were considered, as they provide highly accurate electronic excitation energies.[60–65] The results obtained yielding very similar absorption spectra. Solvation effects were included using the solvation model based on density, SMD. In our previous study, we observed minimal differences in UV-vis absorption values and intensities when comparing the SMD model to the conductor-like polarizable continuum model, C-PCM, and integral equation formalism of the polarizable continuum model, IEFPCM.[45] Acetonitrile was selected as the solvent based on evidence from various studies suggesting that highly polar and aprotic solvents, are the optimal choice for DSSCs, due to their effectiveness in promoting dye adsorption and facilitating electron injection.[66] For modeling the semiconductor, a $(TiO_2)_{14}$ cluster was selected, derived from the crystallographic structure of TiO_2 anatase by cleaving the (1 0 1) surface. The dyes were anchored to the TiO_2 surface by bonding two oxygen atoms from the anchoring group, *e.g.* cyanoacrylate, phosphonate, boron acid, to two titanium atoms. This approach is supported by prior studies that consistently demonstrate the bidentate mode as the most stable binding geometry.[51,61,67,68] It's worth mentioning that the $(TiO_2)_9$ cluster has been shown to be the smallest acceptable model capable of accurately replicating the physical parameters of a real TiO_2 semiconductor. Thus, the size of the cluster proposed here can be considered representative model of TiO_2.[69–71] The geometry optimizations of Dye@$(TiO_2)_{14}$ were conducted using LANL2DZ effective core potential and its accompanying basis set for Ti atom, while the other atoms were treated with the double-ξ basis set 6-31G(d) and the so-called dispersion-corrected B3LYP functional, B3LYP-D3, recommended for accounting for weak interactions, including van der Waals dispersive forces,[72,73] which play a significant role in the adsorption process between the TiO_2 surface and the dye. The solvation effect was considered using the SMD model.

2.1 Theoretical background

The efficiency of dye photosensitizers is determined by their photoelectric conversion efficiency, PCE or η, which measures the amount of sunlight converted into electrical energy by dye. This efficiency can be evaluated using the formula:[74]

$$\eta = \frac{J_{sc} \cdot V_{oc}}{P_{in}} \cdot \mathrm{FF} \quad (1)$$

where P_{in} denotes the incident solar power on the cell, FF represents the fill factor whose value can be approximated using the following equation:[75]

$$\mathrm{FF} = \frac{\frac{e \cdot V_{oc}}{k_B T} - \ln\left(\frac{e \cdot V_{oc}}{k_B T} + 0.72\right)}{\frac{e \cdot V_{oc}}{k_B T} + 1} \quad (2)$$

where e is the elementary charge of the electron, k_B represents the Boltzmann constant at the temperature T (300 K) and V_{oc} is the theoretical estimation of the open-circuit voltage which can be approximated by the following expression:[76]

$$e \cdot V_{oc} = E_{LUMO} - E_{CB} \quad (3)$$

where E_{LUMO} is the LUMO energy of dyes and E_{CB} is the energy of the conduction band of TiO_2

The short circuit current, J_{sc}, is determined using the following expression:[76]

$$J_{sc} = e \cdot \int \mathrm{LHE}(\lambda) \Phi_{inj} \eta_{reg} \eta_{coll} \vartheta_{ph.AM\ 1.5G}(\lambda) \mathrm{d}\lambda \quad (4)$$

the integration occurs within the wavelength range of 280 to 920 nm. In this context $\vartheta_{ph.AM\ 1.5G}$ corresponds to the photon flux under AM 1.5G solar spectra irradiance, Φ_{inj} stands for the electron injection efficiency, η_{reg} is the dye regeneration efficiency and η_{coll} denotes the electron collection efficiency.[45–48] In

Open Access Article. Published on 02 August 2024. Downloaded on 2/7/2026 6:10:27 PM.
This article is licensed under a Creative Commons Attribution-NonCommercial 3.0 Unported Licence.

the optimal condition $\Phi_{inj} = \eta_{reg} = \eta_{coll} = 1$, which is the case we have considered here.

The light harvesting efficiency, LHE, is related to the dye absorption region through the equation:

$$LHE(\lambda) = 1 - 10^{-\varepsilon(\lambda)\Gamma} \quad (5)$$

where $\varepsilon(\lambda)$ represents the molar absorption coefficient at a specific wavelength, while Γ is the surface loading of dye, calculated as the product of dye concentration c and TiO_2 film thickness b. A very low value of 20 nmol cm^{-2} was chosen (the same value is applied in all cases since the molecular sizes vary slightly, with minimal impact on surface coverage) to place us in the most "unfavorable loading conditions", as an increase in this parameter significantly increases the LHE value and consequently J_{sc}.

3. Results and discussion

3.1 Frontiers molecular orbitals analysis and absorption spectra

DSSCs offer a hopeful avenue for maximizing solar energy utilization, where the energy characteristics of the dye sensitizers are pivotal in dictating their efficacy. A fundamental requirement involves ensuring that the LUMO energy level aligns suitably to facilitate the seamless injection of electrons into the conduction band (CB) of the semiconductor. Moreover, achieving an optimal energy level for the HOMO is imperative to ensure efficient electron harvesting. In Fig. 2 an illustrative depiction of the energy landscape pertaining to the molecular orbitals of the analyzed dyes is reported. The presence of the pyrrolic group as an electron donor consistently leads to an increase in the energy value of the HOMO, slightly exceeding −4.8 eV, the redox potential of the electrolyte I^-/I_3^- relative to the vacuum level,[77] in all cases. In greater detail, the impact is significantly accentuated with the introduction of the pentacene group in combination with the cyanoacrylic and phosphonate acceptor groups. While this arrangement may appear to compromise efficient electron recovery, this aspect will be revisited in models where the dyes are adsorbed onto the surface of TiO_2. Every LUMO level resides notably higher than the conduction band CB of TiO_2 (−4.0 eV)[78] exhibiting energy differentials substantially surpassing 0.2 eV. This discrepancy is approximately equivalent to the threshold above which electron injection is thermodynamically favorable.[79]

Comprehending the absorption characteristics of dye sensitizers stands as a pivotal step in enhancing their efficacy within DSSCs. Fig. 3 depicts the UV-vis absorption spectra of the studied dyes, showcasing a prominent peak in the visible region for both acene-unsubstituted and anthracene substituted compounds, characterized by significant intensity due to the HOMO → LUMO transition, suggesting the intramolecular charge transfer, ICT, see Table 1 and Fig. 2. Derivatives featuring the pentacene group exhibit UV absorption beyond 800 nm attributable to ICT transfer, alongside a less pronounced band around 500 nm, contributing to the light harvesting efficiency, LHE, value. A secondary band below 400 nm is also observed in most cases, albeit likely making a minor contribution to LHE considering the low solar irradiance at those wavelengths. In reference to optical properties, moderate effects are observed due to the substitution of the electron-attracting group. For the boronic acid derivatives, **A3**, absorption occurs at a longer wavelength compared to **A1** and **A2** when the acene group is introduced. This shift is due, on one hand, to the hyperconjugation of the aromatic system with the empty p orbital of the boron atom. Additionally, the presence of the boronic acid group can facilitate ICT, significantly affecting the absorption properties and resulting in a red shift due to the new electronic interactions and transitions. In compounds bearing pentacene the phosphonic group, results in absorption at longer wavelengths than the cyanoacrylic derivative, while in derivatives substituted with anthracene, this behavior is reversed. Compared to **SQD**, the absorptions in the visible region of both the unsubstituted and anthracene-substituted

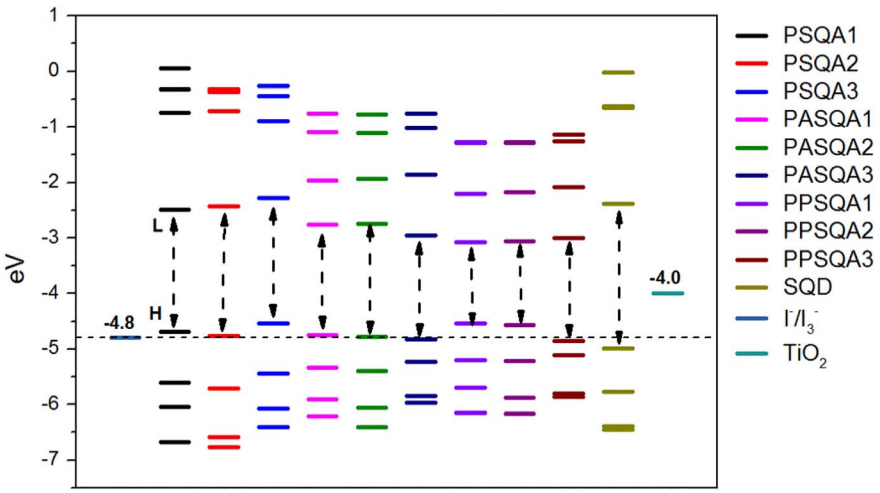

Fig. 2 Selected MOs energy levels in acetonitrile solvent for the designed dyes at B3LYP/6-311+G(2d,p)/SMD level together with **SQD** as reference, TiO_2 CB and I^-/I_3^- redox potential.

© 2024 The Author(s). Published by the Royal Society of Chemistry

Open Access Article. Published on 02 August 2024. Downloaded on 2/7/2026 6:10:27 PM.
This article is licensed under a Creative Commons Attribution-NonCommercial 3.0 Unported Licence.

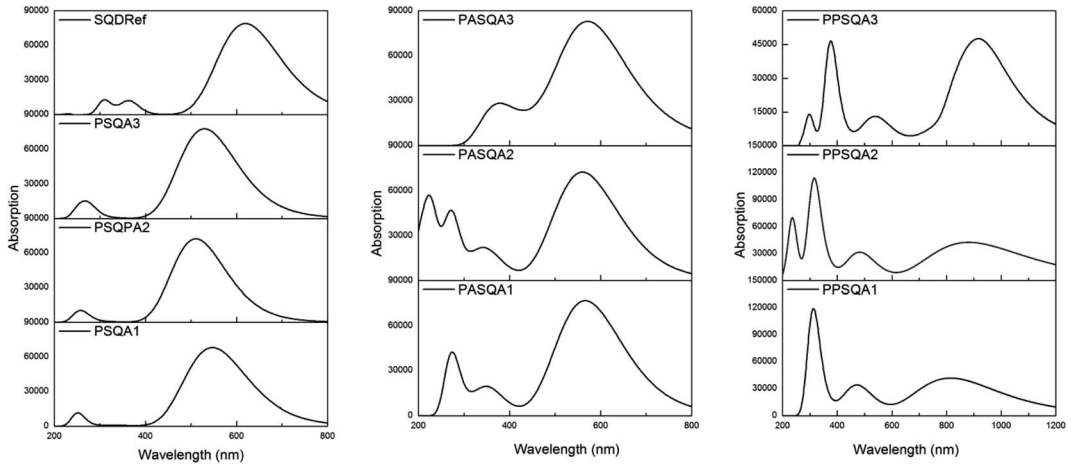

Fig. 3 Absorption spectra of dyes in acetonitrile at TD-CAM-B3LYP/6-311+G(2d,p)/SMD level. The spectra are Gaussian broaded with 0.35 eV (half width half maximum).

dyes occur at shorter wavelengths and exhibit comparable intensity. However, the absorption bands observed below 400 nm show significantly higher intensity than the reference. The UV-vis spectra calculated using ωB97XD and M062X functionals for the most efficient molecules containing anthracene and pentacene closely match the results obtained through the application of CAM-B3LYP, as shown in Fig. S1.†

The simulated light harvesting efficiency curves, see Fig. 4, reflects the characteristics of the UV-vis spectra. It is particularly noted that the **SQD** shows LHE values close to 1 around 600 nm, while the investigated dyes, except for the pentacene-substituted derivatives, exhibit maximum LHE values around 500 nm, which decay more rapidly compared to **SQD**. On the other hand, these compounds better utilize solar irradiance in the region between 400 and 500 nm, where **SQD** has negligible LHE values. The pentacene-substituted derivatives show significant LHE values starting from 700 nm, thus indicating potential use in co-sensitizing with anthracene derivatives,

Table 1 Absorption wavelengths, oscillator strength, main contributions ($f > 0.2$) to the transitions, J_{sc} (mA cm^{-2}), excitation energy E (cm^{-1}) and life-time of the excited state τ (ns) are reported for the dyes in acetonitrile at CAM-B3LYP/6-311+G(2d,p)/SMD level

Compound	λ nm	λ eV	f	Main contribution to the transition	J_{sc}	E	τ
PSQA1	546.95		1.68	H → L (94%)	16.45	18 389.60	2.53
PSQA2	510.66		1.79	H → L (93%)	14.13	18 631.56	2.32
PSQA3	529.44		1.92	H → L (93%)	15.98	25 971.27	1.11
PASQA1	566.21		1.90	H → L (83%)	22.17	17 663.69	2.43
	354.60		0.32	H−2 → L (58%)			
PASQA2	560.10		1.78	H → L (82%)	20.47	17 825.00	2.55
PASQA3	598.11		0.64	H → L (22%)	18.44		
	562.56		1.42	H → L+1 (88%)		25 003.40	1.62
	442.94		0.26	H−1 → L+1 (68%)			
	378.89		0.42	H−1 → L+2 (36%)			
PPSQA1	814.98		1.03	H → L (96%)	24.81	12 259.73	9.30
	484.52		0.58	H → L+1 (78%)			
	453.50		0.21	H−1 → L (78%)			
	361.45		0.24	H → L+2 (82%)			
	331.20		0.22	H−2 → L+1 (79%)			
	311.80		2.61	H → L+4 (50%)			
PPSQA2	881.06		1.05	H → L (97%)	23.15	11 372.50	10.60
	486.88		0.55	H−1 → L (60%)			
	474.11		0.22	H → L+1 (53%)			
	364.40		0.27	H → L+2 (78%)			
	318.61		0.74	H−2 → L+1 (42%)			
	315.12		1.70	H → L+4 (38%)			
PPSQA3	918.44		1.15	H → L+1 (66%)	22.78	21 615.84	2.68
	376.03		1.06	H → L+2 (52%)			
SQD	622.13		1.95	H → L (97%)	19.06	18 147.60	2.24

Open Access Article. Published on 02 August 2024. Downloaded on 2/7/2026 6:10:27 PM.
This article is licensed under a Creative Commons Attribution-NonCommercial 3.0 Unported Licence.

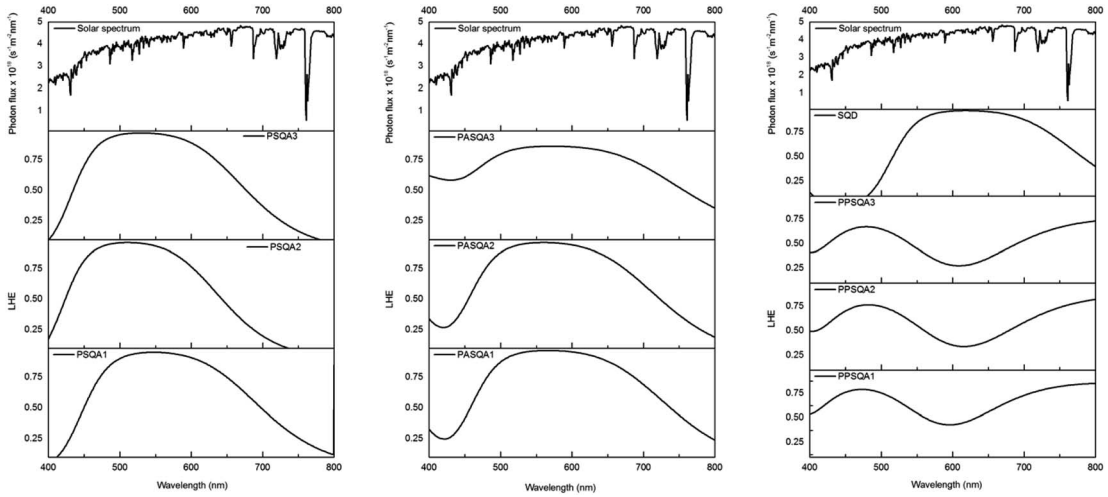

Fig. 4 LHE (λ) curves of selected dyes ($\Gamma = 20$ nmol cm^{-2} is taken in all cases). AM 1.5G solar spectrum is reported in grey.

resulting in a panchromatic effect that spans extensively from 400 to well beyond 920 nm into the NIR region. The short circuit photocurrent is a critical performance metric for DSSC devices and is directly proportional to light harvesting efficiency value, as determined by the eqn (4) provided above. Under optimal conditions, where the injection efficiency and the charge collection efficiency are both equal to 1, the J_{sc} values listed in Table 1 are obtained. These results demonstrate that incorporating the acene group enhances the performance of this indicator. Specifically, the pentacene group yields the best results compared to anthracene group. The highest J_{sc} values are obtained when the acene group is combined with anchoring group **A1**. However, significant results are also achieved with **A2** and **A3**, particularly considering that all dyes featuring acene moieties exhibit higher J_{sc} values compared to the reference, for which we calculated a value of 19.06 mA cm^{-2}.

Fig. 5 illustrates the spatial arrangement of the frontier molecular orbitals, showing electron density transition *via* the π-linker from the dye-donor region in the HOMO to the acceptor region in the LUMO, thereby promoting the ICT process. The overlap between the HOMO and LUMO orbitals along the π-linker indicates strong induction and electron-withdrawing capabilities of both donor and acceptor components, thereby further enhancing the charge transfer.

The lifetime of the excited state, τ, is another crucial factor in determining the efficiency of charge injection to TiO_2. A longer excited state lifetime allows the dye to remain in its cationic form for an extended period, which is beneficial for charge transfer. This prolongation will retard the charge recombination process increasing the efficiency of charge collection thus enhancing the performance of DSSCs.[80–82] τ can be calculated using the following equation:

$$\tau = 1.499/(f \cdot E^2)$$

where E represents the excitation energy of the different electronic states (in cm^{-1}) and f is the oscillator strength of the electronic state. The computed values of τ for all investigated dyes are presented in Table 1.

According to the table, with the exception of the boronic acid derivatives, the dyes with the pentacene group maintain their cationic state longer, about four times longer than **SQD**, resulting in higher charge transfer efficiency and improved DSSC performance. The **A3** anchoring group plays a negative role, likely due to the presence of the boron atom, a Lewis acid, which significantly destabilizes the cationic form. The anthracene group provides performance comparable to the reference.

3.2 TiO_2-dye adsorption

To analyze the electron transfer mechanism at the interface, we concentrated on the adsorption complexes on surface semiconductor. In every scenario, we examined the bidentate bridging configuration, recognized as the most stable adsorption mode for carboxylic, phosphonic and boronic acid groups as evidenced by previous studies.[51–54] This model posits that the sensitizer attaches to the semiconductor *via* two O–Ti bonds, while the proton from the acid group is transferred to the nearest double-coordinated oxygen atom on the surface. The calculated adsorption energies, presented in Table 2, reveal robust interactions between the dyes and the TiO_2 surface. Consistent with literature the phosphonic derivatives exhibit the highest adsorption energy values, followed by the cyanoacrylic group and the boronic acid derivative. The adsorption energies are evaluated as follows:

$$E_{ads} = E_{Dye@TiO_2} - (E_{TiO_2} + E_{Dye})$$

Fig. 6 presents the Partial Density of States (PDOS) for the dyes@TiO_2 interfaces. Upon adsorption, the LUMO energy levels of all sensitizers are consistently located above the conduction band of TiO_2, ensuring an adequate driving force for electron injection into the semiconductor's conduction band, see Table 2. Additionally, the HOMO energy levels shift to lower values after adsorption, increasing the energy difference

© 2024 The Author(s). Published by the Royal Society of Chemistry

Open Access Article. Published on 02 August 2024. Downloaded on 2/7/2026 6:10:27 PM.
This article is licensed under a Creative Commons Attribution-NonCommercial 3.0 Unported Licence.

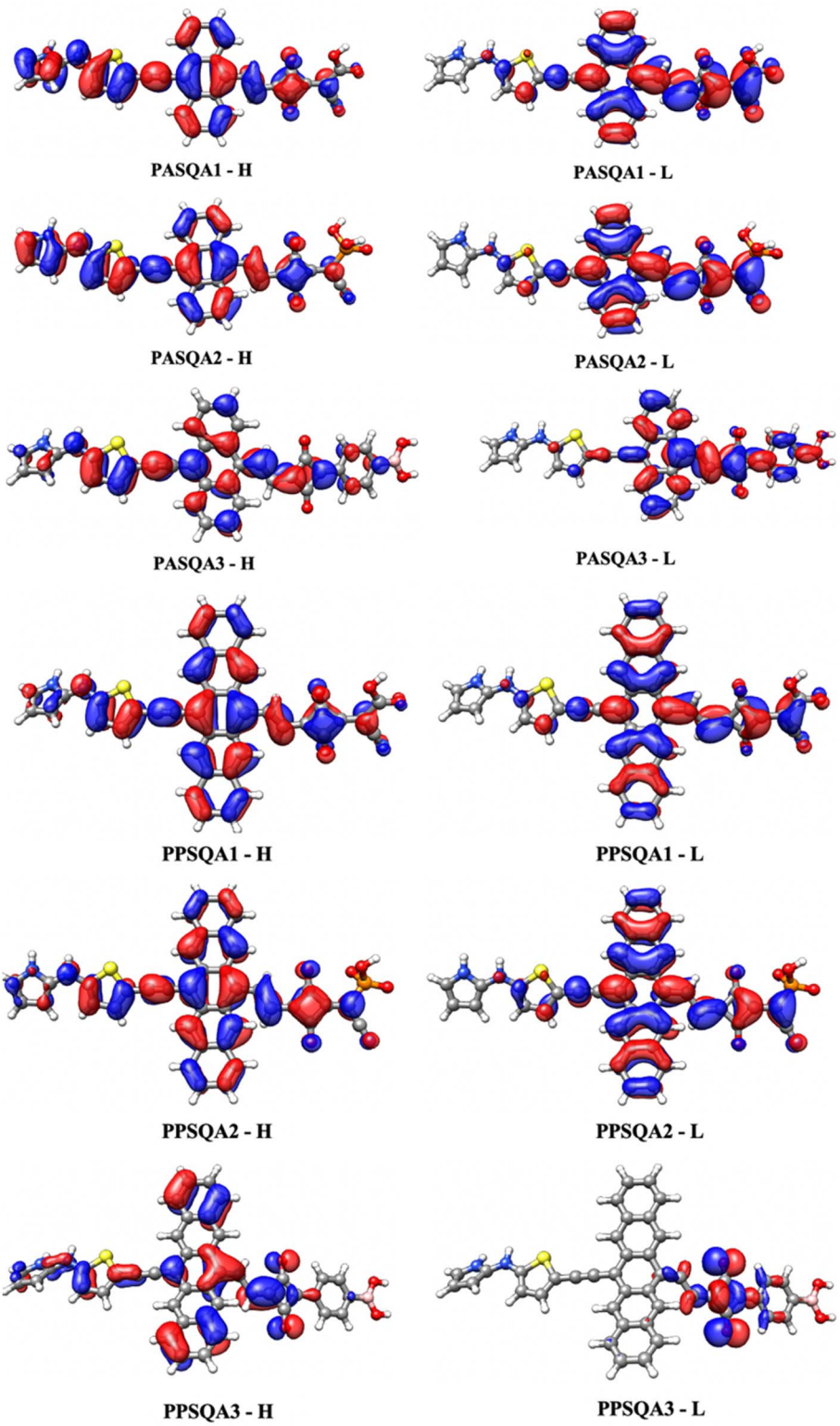

Fig. 5 Frontiers molecular orbitals of HOMO and LUMO of the dyes in acetonitrile at TD-CAM-B3LYP/6-311+G(2d,p)/SMD level. The surfaces are generated with an iso value at 0.02.

relative to the electrolyte redox potential (−4.8 eV). This shift supports favorable ground-state dye regeneration, which significantly enhances the open-circuit voltage and thus the overall device performance. Prior to adsorption, the examined dyes exhibit positive ΔG^{reg} values, indicating that the regeneration process is thermodynamically unfavorable for these sensitizers. After adsorption efficient dye regeneration are obtained, ΔG^{reg} values become negative and within the range of

Open Access Article. Published on 02 August 2024. Downloaded on 2/7/2026 6:10:27 PM. This article is licensed under a Creative Commons Attribution-NonCommercial 3.0 Unported Licence.

Table 2 Adsorption energies, E_{ads}, energy levels and driving forces for the investigates dyes@TiO_2 complexes (energies in eV)

Compound	E_{ads}	HOMO	LUMO	ΔG^{inj}	ΔG^{reg} [a]	V_{oc}	FF	PCE (%)
PASQA1@TiO_2	−0.87	−5.14	−2.51	−1.07	−0.34	1.49	0.913	30.16
PASQA2@TiO_2	−3.01	−5.13	−2.47	−1.08	−0.35	1.53	0.915	28.66
PASQA3@TiO_2	−0.81	−5.12	−2.24	−1.08	−0.32	1.76	0.924	29.99
PPSQA1@TiO_2	−0.84	−5.06	−2.36	−0.46	−0.26	1.64	0.920	37.43
PPSQA2@TiO_2	−2.97	−5.08	−2.45	−0.33	−0.28	1.55	0.916	32.87
PPSQA3@TiO_2	−0.77	−5.10	−2.36	−0.25	−0.30	1.64	0.920	34.37
SQD@TiO_2	−0.85	−5.07	−2.57	−0.73	−0.27	1.43	0.910	24.82

[a] $\Delta G^{reg} = E^{redox\text{-}electrolyte} - E^{ox\text{-}dye}$.

−0.26–0.35 eV. ΔG^{inj} is the free energy involved in the electron injection process, and is given by:

$$\Delta G^{inj} = E^{ox\text{-}dye*} - E_{CB}$$

where E_{CB} is the reduction potential of the TiO_2 conduction band (4.0 eV) whereas $E^{ox\text{-}dye*}$ is the oxidation potential of the dye in its excited state and can be computed as:

$$E^{ox\text{-}dye*} = E^{ox\text{-}dye} - E_{0\text{–}0}$$

Here $E^{ox\text{-}dye}$ is the oxidation potential of the dye in its ground state and $E_{0\text{–}0}$ is the vertical electronic transition energy corresponding to $\lambda_{max.}$ Generally, lower ΔG^{inj} values indicate higher efficiency in electron injection.

The UV-vis spectra recalculated after adsorption onto the surface show a red-shift of the bands compared to the free dyes,

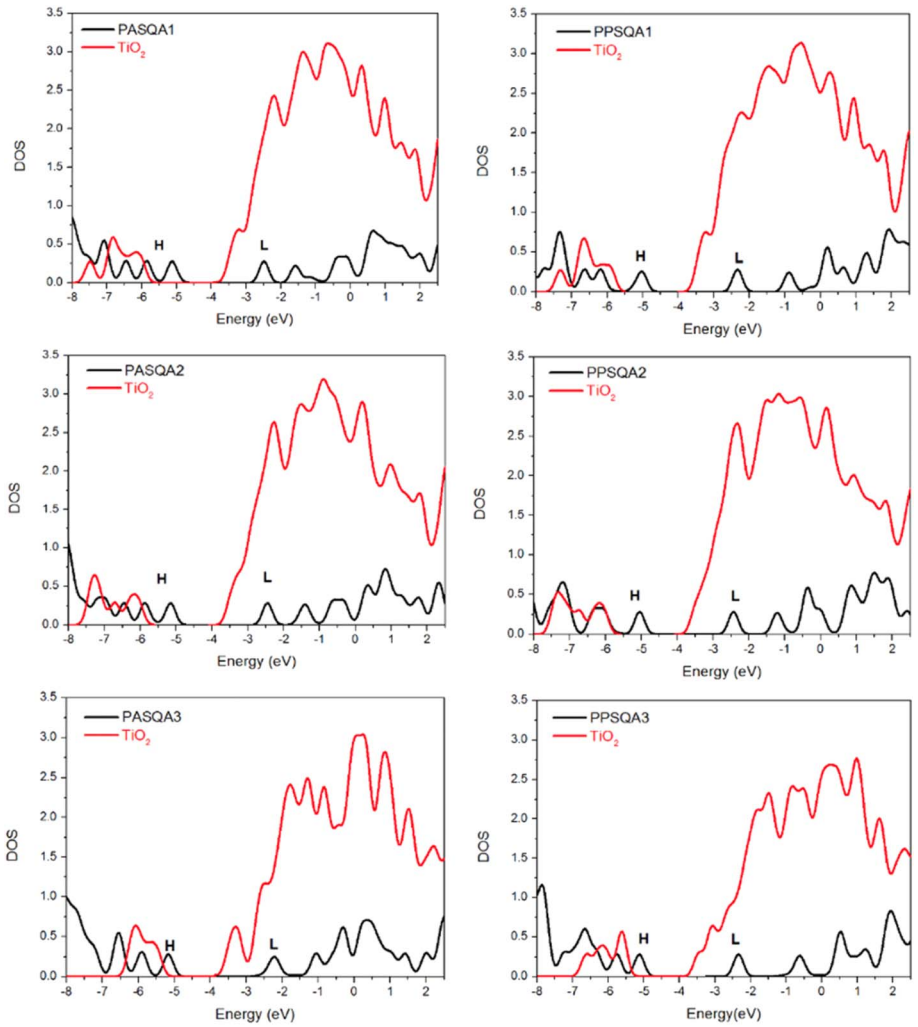

Fig. 6 Calculated PDOS for **PASQA1**, **PASQA2**, **PASQA3**, **PPSQA1**, **PPSQA2** and **PPSQA3**.

© 2024 The Author(s). Published by the Royal Society of Chemistry

Open Access Article. Published on 02 August 2024. Downloaded on 2/7/2026 6:10:27 PM.
This article is licensed under a Creative Commons Attribution-NonCommercial 3.0 Unported Licence.

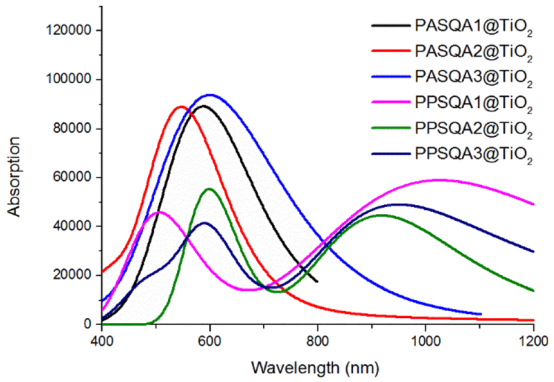

Fig. 7 Absorption spectra in acetonitrile of dyes@TiO_2 at TD-CAM-B3LYP/6-31G(d)/LANL2DZ/SMD level. The spectra are Gaussian broaded with 0.35 eV (half width half maximum).

see Fig. 7. The natural transition orbitals of the dyes after binding with TiO_2 are shown in Fig. S2.† Main contributions to the S0 → S1 transition indicate that the HOMO and LUMO levels of dyes@TiO_2 are localized to the sensitizers, retaining the character of the isolated dyes. Most of the LUMO+n levels (where $n \geq 4$) are centered on the substrate and exhibit the same characteristics as TiO_2, indicating no coupling with the semiconductor's conduction band. Interacting orbitals are observed at the L+1, L+2, and L+3 energy levels, see Fig. S2,† showing that electron distribution is delocalized between the dyes and the TiO_2 surface, which signifies electron transfer to the semiconductor *via* the anchoring group, resulting in direct electron transfer.

Considering the values reported in Table 2, it is observed that all the investigated dyes exhibit better performance than the reference, with the introduction of the pentacene group increasing the efficiency by over 50% compared to **SQD**.

4. Conclusions

We performed an extensive DFT study on the spectroscopic and photoelectric characteristics of newly designed squaraine-based dyes. These molecules feature a donor group made up of 2-amino pyrrole, an acene group positioned near the donor, and three distinct anchoring groups: cyanoacrylate, **A1**, phosphonate, **A2**, and a boronic acid derivative, **A3**. UV-vis data indicate that dyes with pentacene exhibit excellent absorption properties extending beyond 920 nm, which significantly enhances the panchromatic effect. These dyes also have longer excited-state lifetimes than the reference **SQD**, with pentacene-containing dyes featuring **A1** or **A2** groups showing lifetimes about four times longer, which improves charge transfer. Conversely, the boronic acid derivatives exhibited shorter excited-state lifetimes than the reference, indicating impaired charge transfer despite their superior optical properties. The most promising results were obtained with dyes containing pentacene combined with **A1** or **A2** anchoring groups. Notably, dyes featuring **A1** exhibited the highest J_{sc} and PCE values in their series. Phosphonate derivatives showed the highest energy adsorption on the surface and significant V_{oc}, J_{sc} and PCE values. All dyes demonstrated efficient electron recovery after adsorption on TiO_2, with HOMO levels dropping significantly below −4.8 eV. The dyes effectively inject electrons into the TiO_2 conduction band, supported by favorable ΔG^{inj} and ΔG^{reg} values, ensuring easy regeneration. These findings highlight the potential of the designed dyes for use as standalone sensitizers or in co-sensitizing configurations. Their panchromatic characteristics, with absorption extending into the NIR region, offer significant promise for advancing photovoltaic technologies.

Data availability

The code for Gaussian 16 can be found at **https://gaussian.com/gaussian16/**. The revision of the code employed for this study is C.01 as implemented on hardware Galileo100 system of Cineca Italian SuperComputing Resource Allocation (**https://www.hpc.cineca.it/systems/software/scientific-field/chemistry/gaussian-g16/**).

Author contributions

Giuseppe Consiglio: conceptualization, methodology, investigation, writing, revision and editing. Adam Gorczyński: investigation, writing, revision and editing. Guido Spoto: methodology, writing, revision and editing. Salvatore Petralia: investigation, writing, revision and editing. Giuseppe Forte: conceptualization, supervision, methodology, writing original draft.

Conflicts of interest

The authors declare no conflicts of interest.

Acknowledgements

This work has been partially funded by European Union (NextGeneration EU), through the National Centre for HPC, Big Data and Quantum Computing (E63C22001000006) and by Class B project, code HP10BOPIYD, supported by Cineca Italian SuperComputing Resource Allocation.

References

1 S. Shalini, R. Balasundaraprabhu, T. Satish Kumar, N. Prabavathy, S. Senthilarasu and S. Prasanna, *Int. J. Energy Res.*, 2016, **40**, 1303–1320.
2 M. K. Nazeeruddin, P. Pechy and M. Grätzel, *Chem. Commun.*, 1997, 1705–1706.
3 M. K. Nazeeruddin, P. Pechy, T. Renouard, S. M. Zakeeruddin, R. Humphry-Baker, P. Comte, P. Liska, L. Cevey, E. Costa, V. Shklover, L. Spiccia, G. D. Deacon, C. A. Bignozzi and M. Grätzel, *J. Am. Chem. Soc.*, 2001, **123**, 1613–1624.
4 R. Buscaino, C. Baiocchi, C. Barolo, C. Medana, M. Grätzel, M. K. Nazeeruddin and G. Viscardi, *Inorg. Chim. Acta*, 2008, **361**, 798–805.

© 2024 The Author(s). Published by the Royal Society of Chemistry

Open Access Article. Published on 02 August 2024. Downloaded on 2/7/2026 6:10:27 PM. This article is licensed under a Creative Commons Attribution-NonCommercial 3.0 Unported Licence.

5 J. F. Huang, J. M. Liu, P. Y. Su, Y. F. Chen, Y. Shen, L. M. Xiao, D. B. Kuang and C. Y. Su, *Electrochim. Acta*, 2015, **174**, 494–501.
6 Z. Z. Lu, J. Peng, W. De, C. H. Lin, C. G. Wu, K. C. Ho, Y. C. Lin and K. L. Lu, *Eur. J. Inorg. Chem.*, 2016, 1214–1224.
7 A. Yella, H. W. Lee, H. N. Tsao, C. Yi, A. K. Chandiran, M. K. Nazeeruddin, E. W. G. Diau, C. Y. Yeh, S. M. Zakeeruddin and M. Grätzel, *Science*, 2011, **334**, 629–634.
8 S. Mathew, A. Yella, P. Gao, R. Humphry-Baker, B. F. Curchod, N. Ashari-Astani, I. Tavernelli, U. Rothlisberger, M. K. Nazeeruddin and M. Grätzel, *Nat. Chem.*, 2014, **6**, 242–247.
9 G. Consiglio, S. Failla, C. G. Fortuna, L. D'Urso and G. Forte, *Comput. Theor. Chem.*, 2015, **1067**, 1–6.
10 S. Aghazada, P. Gao, A. Yella, G. Marotta, T. Moehl, J. Teuscher, J. E. Moser, F. De Angelis, M. Grätzel and M. K. Nazeeruddin, *Inorg. Chem.*, 2016, **55**, 6653–6659.
11 N. V. Krishna, J. V. S. Krishna, M. Mrinalini, S. Prasanthkumar and L. Giribabu, *ChemSusChem*, 2017, **10**, 4668–4689.
12 I. P. Oliveri, G. Forte, G. Consiglio, S. Failla and S. Di Bella, *Inorg. Chem.*, 2017, **56**, 14206–14213.
13 C. C. Chen, J. S. Chen, V. S. Nguyen, T. C. Wei and C. Y. Yeh, *Angew. Chem.*, 2021, **60**(9), 4886–4893.
14 G. Chen, H. Sasabe, T. Igarashi, Z. Hong and J. Kido, *J. Mater. Chem. A*, 2015, **3**, 14517–14534.
15 S. Sreejith, P. Carol, P. Chithra and A. Ajayaghosh, *J. Mater. Chem.*, 2008, **18**, 264–274.
16 L. Venkataraman, J. E. Klare, C. Nuckolls, M. S. Hybertsen and M. L. Steigerwald, *Nature*, 2006, **7105**, 904–907.
17 Y. T. Fu, D. A. da Silva Filho and G. Sini, *Adv. Funct. Mater.*, 2014, **24**, 3790–3798.
18 Y. S. Yen, H. H. Chou, Y. C. Chen, C. Y. Hsu and J. T. Lin, *J. Mater. Chem.*, 2012, **18**, 8734–8747.
19 P. Ruankham, L. Macaraig, T. Sagawa, H. Nakazumi and S. Yoshikawa, *J. Phys. Chem. C*, 2011, **48**, 23809–23816.
20 Y. Ooyama and Y. Harima, *Eur. J. Org. Chem.*, 2009, **18**, 2903–2934.
21 A. Mishra, M. K. R. Fischer and P. Bäuerle, *Angew. Chem., Int. Ed.*, 2009, **14**, 2474–2499.
22 A. G. Al-Sehemi, A. Irfan, A. M. Asiri and Y. A. Ammar, *Spectrochim. Acta, Part A*, 2012, **91**, 239–243.
23 A. G. Al-Sehemi, A. Irfan, A. M. Asiri and Y. A. Ammar, *J. Mol. Struct.*, 2012, **1019**, 130–134.
24 C. Bonaccorso, F. De Rossi, M. Panigati, C. G. Fortuna, G. Forte, T. M. Brown, G. m. Farinola and G. Musumarra, *Tetrahedron*, 2015, **71**, 7260–7266.
25 S. A. Al-horaibi, S. T. Gaikwad and A. S. Rajbhoj, *Adv. Mater. Lett.*, 2018, **9**, 275–283.
26 D. Yang, T. Sano, H. Sasabe and J. Kidoa, *Dyes Pigm.*, 2019, **163**, 564–572.
27 L. Zhang and J. M. Cole, *J. Mater. Chem. A*, 2017, **5**, 19541–19559.
28 V. Punitharasu, M. F. M. Kavungathodi, A. K. Singh and J. Nithyanandhan, *ACS Appl. Energy Mater.*, 2019, **2**, 8464–8472.
29 Y. Chiba, A. Islam, Y. Watanabe, R. Komiya, N. Koide and L. Han, *Jpn. J. Appl. Phys., Part 1*, 2006, **45**, L638.
30 H. Tian, X. Yang, R. Chen, A. Hagfeldt and L. Sun, *Energy Environ. Sci.*, 2009, **2**, 674–677.
31 J. H. Yum, E. Baranoff, S. Wenger, M. K. Nazeeruddin and M. Grätzel, *Energy Environ. Sci.*, 2011, **4**, 842–857.
32 N. Koumura, Z. S. Wang, S. Mori, M. Miyashita, E. Suzuki and K. Hara, *J. Am. Chem. Soc.*, 2006, **128**, 14256–14257.
33 C. Qin, A. Islam and L. Han, *Dyes Pigm.*, 2012, **94**, 553–560.
34 S. Qu, C. Qin, A. Islam, J. Hua, H. Chen, H. Tian and L. Han, *Chem.–Asian J.*, 2012, **7**, 2895–2903.
35 A. Ehret, L. Stuhl and M. Spitler, *J. Phys. Chem. B*, 2001, **105**, 9960–9965.
36 R. Y. Ogura, S. Nakane, M. Morooka, M. Orihashi, Y. Suzuki and K. Noda, *Appl. Phys. Lett.*, 2009, **94**, 073308.
37 A. Islam, T. Swetha, M. R. Karim, M. Akhtaruzzaman, L. Han and S. P. Singh, *Phys. Status Solidi A*, 2015, **212**, 651–656.
38 C. M. Lan, H. P. Wu, T. Y. Pan, C. W. Chang, W. S. Chao, C. T. Chen, C. L. Wang, C. Y. Lin and E. W. G. Diau, *Energy Environ. Sci.*, 2012, **5**, 6460–6464.
39 J. Chang, C. P. Lee, D. Kumar, P. W. Chen, L. Y. Lin, K. J. Thomas and K. C. Ho, *J. Power Sources*, 2013, **240**, 779–785.
40 S. Zhang, A. Islam, X. Yang, C. Qin, K. Zhang, Y. Numata, H. Chen and L. Han, *J. Mater. Chem. A*, 2013, **1**, 4812–4819.
41 Y. Xie, Y. Tang, W. Wu, Y. Wang, J. Liu, X. Li, H. Tian and W. H. Zhu, *J. Am. Chem. Soc.*, 2015, **137**, 14055–14058.
42 K. Pei, Y. Wu, H. Li, Z. Geng, H. Tian and W. H. Zhu, *ACS Appl. Mater. Interfaces*, 2015, **7**, 5296–5304.
43 A. Islam, M. Akhtaruzzaman, T. H. Chowdhury, C. Qin, L. Han, I. M. Bedja, R. Stalder, K. S. Schanze and J. R. Reynolds, *ACS Appl. Mater. Interfaces*, 2016, **8**, 4616–4623.
44 A. Islam, T. H. Chowdhury, C. Qin, L. Han, J. J. Lee, I. M. Bedja, M. Akhtaruzzaman, K. Sopian, A. Mirloupe and N. Leclerc, *Sustainable Energy Fuels*, 2018, **2**, 209–214.
45 G. Consiglio, A. Gorczynski, S. Petralia and G. Forte, *RSC Adv.*, 2023, **13**, 1019–1030.
46 G. Consiglio, A. Gorczynski, S. Petralia and G. Forte, *Dalton Trans.*, 2023, **52**, 15995–16004.
47 G. Consiglio, A. Gorczynski, S. Petralia and G. Forte, *J. Mater. Chem. C*, 2024, **12**, 903–912.
48 G. Consiglio, A. Gorczynski, G. Spoto, S. Petralia and G. Forte, *New J. Chem.*, 2024, **48**, 10026–10037.
49 S. A. Al-horaibi, A. B. Al-Odayni, A. Alezzy, M. Al-Saeedy, W. Saeed, A. Hasan and R. M. El-Shishtawy, *J. Mol. Struct.*, 2023, **1292**, 136130.
50 S. Shaban, A. K. Vats and S. S. Pandey, *Molecules*, 2023, **28**(6), 2784.
51 C. O'Rourke and D. R. Bowler, *J. Phys.: Condens.Matter*, 2014, **26**, 195302.
52 L. Zhang and J. M. Cole, *ACS Appl. Mater. Interfaces*, 2015, **7**, 3427–3455.
53 Q. Zhang, S. Wei, S. Zhou, X. Wei, Z. Xu, Z. Wang, B. Wei and X. Lu, *ACS Appl. Electron. Mater.*, 2020, **2**, 2141–2150.
54 D. Fadili, S. M. Bouzzine and M. Hamidi, *New J. Chem.*, 2021, **45**, 2723–2733.

© 2024 The Author(s). Published by the Royal Society of Chemistry

Open Access Article. Published on 02 August 2024. Downloaded on 2/7/2026 6:10:27 PM. This article is licensed under a Creative Commons Attribution-NonCommercial 3.0 Unported Licence.

55 B. Sekaran and R. Misra, *Coord. Chem. Rev.*, 2022, **453**, 214312.
56 G. Forte, A. La Magna, I. Deretzis and R. Pucci, *Nanoscale Res. Lett.*, 2010, **5**, 158–163.
57 M. J. Frisch, G. W. Trucks, H. B. Schlegel, G. E. Scuseria, M. A. Robb, J. R. Cheeseman, G. Scalmani, V. Barone, G. A. Petersson, H. Nakatsuji, X. Li, M. Caricato, A. V. Marenich, J. Bloino, B. G. Janesko, R. Gomperts, B. Mennucci, H. P. Hratchian, J. V. Ortiz, A. F. Izmaylov, J. L. Sonnenberg, D. Williams-Young, F. Ding, F. Lipparini, F. Egidi, J. Goings, B. Peng, A. Petrone, T. Henderson, D. Ranasinghe, V. G. Zakrzewski, J. Gao, N. Rega, G. Zheng, W. Liang, M. Hada, M. Ehara, K. Toyota, R. Fukuda, J. Hasegawa, M. Ishida, T. Nakajima, Y. Honda, O. Kitao, H. Nakai, T. Vreven, K. Throssell, J. A. Montgomery Jr, J. E. Peralta, F. Ogliaro, M. J. Bearpark, J. J. Heyd, E. N. Brothers, K. N. Kudin, V. N. Staroverov, T. A. Keith, R. Kobayashi, J. Normand, K. Raghavachari, A. P. Rendell, J. C. Burant, S. S. Iyengar, J. Tomasi, M. Cossi, J. M. Millam, M. Klene, C. Adamo, R. Cammi, J. W. Ochterski, R. L. Martin, K. Morokuma, O. Farkas, J. B. Foresman, and D. J. Fox, *Gaussian 16 Rev C.01*, Gaussian, Inc., Wallingford CT, 2016.
58 D. Keil, H. Hartmann and T. Moschny, *Dyes Pigm.*, 1991, **17**, 19–27.
59 K. Y. Law, *J. Phys. Chem.*, 1987, **91**, 5184–5193.
60 D. Fadili, S. M. Bouzzine and M. Hamidi, *J. Comput. Electron.*, 2020, **19**, 1629–1644.
61 D. Fadili, S. M. Bouzzine and M. Hamidi, *New J. Chem.*, 2021, **45**, 2723–2733.
62 P. N. Samanta, D. Majumdar, S. Roszak and J. Leszczynski, *J. Phys. Chem. C*, 2020, **124**(5), 2817–2836.
63 Y. Zhao and D. G. Truhlar, *Theor. Chem. Acc.*, 2008, **120**, 215–241.
64 J. D. Chai and M. Head-Gordon, *Phys. Chem. Chem. Phys.*, 2008, **10**, 6615–6620.
65 Y. M. Hailu, M. T. Nguyen and J. C. Jiang, *Phys. Chem. Chem. Phys.*, 2018, **20**, 23564–23577.
66 K. M. Lee, V. Suryanarayanan and K. C. Ho, *J. Power Sources*, 2009, **188**, 635–641.
67 D. Fadili, Z. M. E. Fahim, S. M. Bouzzine, O. T. Alaoui and M. Hamidi, *Comput. Theor. Chem.*, 2022, **1210**, 113645.
68 M. Wagstaffe, A. G. Thomson, M. J. Jackman, M. Torres-Molina, K. L. Syres and K. Handrup, *J. Phys. Chem. C*, 2016, **120**, 1693–1700.
69 R. Sánchez-de-Armas, M. A. San Miguel, J. Oviedo and J. F. Sanz, *Phys. Chem. Chem. Phys.*, 2012, **14**, 225–233.
70 S. de-Armas, M. A. San-Miguel, J. Oviedo, A. Márquez and J. F. Sanz, *Phys. Chem. Chem. Phys.*, 2011, **13**, 1506–1514.
71 R. Sánchez-de-Armas, J. OviedoLópez, M. A. San-Miguel, J. F. Sanz, P. Ordejón and M. Pruneda, *J. Chem. Theory Comput.*, 2010, **6**, 2856–2865.
72 S. T. Schneebeli, A. D. Bochevarov and R. A. Friesner, *J. Chem. Theory Comput.*, 2011, **7**(3), 658–668.
73 E. F. Grossman, D. A. Daramola and amd G. G. Botte, *Chem.–Eur. J.*, 2021, **10**(3), 316–326.
74 M. Grätzel, *Acc. Chem. Res.*, 2009, **42**, 1788–1798.
75 M. A. Green, *Solid-State Electron.*, 1981, **24**, 788–789.
76 T. Zhang, W. Guan, S. Wen, T. Ma, L. Yan and Z. Su, *J. Phys. Chem. C*, 2014, **118**, 29623–29628.
77 J. Preat, A. Hagfeldt and E. A. Perpete, *Energy Environ. Sci.*, 2011, **4**, 4537–4549.
78 J. B. Asbury, Y. Q. Wang, E. C. Hao, H. N. Ghosh and T. Q. Lian, *Res. Chem. Intermed.*, 2001, **27**, 393–406.
79 H. W. Ham and Y. S. Kim, *Thin Solid Films*, 2010, **518**, 6558–6563.
80 Y. Mu, H. D. G. Wu, Z. Shen, S. Li and M. Zhang, *J. Mater. Chem. A*, 2018, **6**(21), 493–500.
81 R. Li, M. Zhang, C. Yan, Z. Yao, J. Zhang and P. Wang, *ChemSusChem*, 2015, **8**, 97–104.
82 Z. Yao, M. Zhang, R. Li, L. Yang, Y. Qiao and P. Wang, *Angew Chem. Int. Ed. Engl.*, 2015, **54**, 5994–5998.

© 2024 The Author(s). Published by the Royal Society of Chemistry